Published in final edited form as:
Biochim Biophys Acta. 2013 August ; 1828(8): 1786–1793. doi:10.1016/j.bbamem.2013.03.008.

Glycerol modulates water permeation through *Escherichia coli* aquaglyceroporin GlpF

Liao Y. Chen*
Department of Physics, University of Texas at San Antonio, One UTSA Circle, San Antonio, TX, 78249, USA

Liao Y. Chen: Liao.Chen@utsa.edu

Abstract

Among aquaglyceroporins that transport both water and glycerol across the cell membrane, *Escherichia coli* glycerol uptake facilitator (GlpF) is the most thoroughly studied. However, one question remains: Does glycerol modulate water permeation? This study answers this fundamental question by determining the three-dimensional potential of mean force of glycerol along the permeation path through GlpF's conducting pore. There is a deep well near the Asn-Pro-Ala (NPA) motifs (6.5 kcal/mol below the bulk level) and a barrier near the selectivity filter (10.1 kcal/mol above the well bottom). This profile owes its existence to GlpF's perfect steric arrangement: The glycerol-protein van der Waals interactions are attractive near the NPA but repulsive elsewhere in the conducting pore. In light of the single-file nature of waters and glycerols lining up in GlpF's amphipathic pore, it leads to the following conclusion: Glycerol modulates water permeation in the μM range. At mM concentrations, GlpF is glycerol-saturated and a glycerol residing in the well occludes the conducting pore. Therefore, water permeation is fully correlated to glycerol dissociation that has an Arrhenius activation barrier of 6.5 kcal/mol. Validation of this theory is based on the existent *in vitro* data, some of which have not been given the proper attention they deserved: The Arrhenius activation barriers were found to be 7 kcal/mol for water permeation and 9.6 kcal/mol for glycerol permeation; The presence of up to 100 mM glycerol did not affect the kinetics of water transport with very low permeability, in apparent contradiction with the existent theories that predicted high permeability (0 M glycerol).

Keywords

Aquaglyceroporin; Chemical potential; Glycerol; Transport; Activation barrier

1. Introduction

Escherichia coli aquaglyceroporin GlpF is a member of the membrane proteins responsible for water and solute transport across the cell membrane [1–6]. Among the aquaglyceroporin sub-family of proteins that conduct both water and glycerol, GlpF is the most thoroughly studied, both in vitro [7–19] and *in silico* [18,20–29]. There is no controversy over the science that GlpF conducts both water and glycerol and how the amphipathic pore of GlpF selectively facilitates the passage of waters and glycerols lining up in a single file through the conducting channel [17,18,20,21]. However, one fundamental question remains: Does

*Tel.: +1 210 458 5457.

Appendix A. Supplementary data: Supplementary data to this article can be found online at http://dx.doi.org/10.1016/j.bbamem.2013.03.008.

glycerol modulate water permeation through GlpF? And, related to this question, there are some unsolved issues about water permeation through this protein's conducting pore: The in vitro data indicate that GlpF is much less permeable to water than *E. coli* aquaporin Z (AQPZ) and other water-selective aquaporins are [13,14,30], but theoretical studies predict that GlpF is more permeable than AQPZ etc. [23,31]; The *in vitro* experiments show that water permeation has an Arrhenius activation barrier that is about 7 kcal/mol [13], but the theoretical studies all give a rather flat free-energy profile throughout the permeation channel of GlpF [20,27]. While the *in vitro* experiments indicate that the presence of up to 100 mM glycerol does not affect the kinetics of water transport [13], all *in silico* studies are limited to 0 M glycerol concentration. All these problems can be resolved once we have an accurate determination of the three-dimensional (3D) potential of mean force (PMF)[32–34] of glycerol as a function of its center-of-mass (COM) coordinates along a path leading from the periplasm to the entry vestibule of GlpF, through the channel, to the cytoplasm. This chemical-potential profile in terms of the 3D PMF, considered on the basis of the structure information available in the literature [17,18], can ascertain the conclusion that glycerol strongly modulates water permeation through GlpF.

Inside the GlpF channel, waters and glycerols line up in a single file, occluding one another from occupying the same *z*-coordinate. (The z-axis is chosen as normal to the membrane-water interface, pointing from the periplasm to the cytoplasm.) Therefore, waters and glycerols permeate through the amphipathic pore of GlpF in a concerted, collective diffusion, driven or not driven by the osmotic pressure. If a deep enough chemical-potential well exists inside the channel (where the chemical potential is lower than the periplasm/cytoplasm bulk level), a glycerol molecule will be bound there, with a probability determined by the glycerol concentration and the dissociation constant. The bound glycerol will occlude permeation of waters and other glycerols through the channel. GlpF will switch between being open and closed to water permeation as a glycerol is dissociated from and bound to the binding site inside the protein's conducting pore. Therefore, such a chemical-potential profile means that glycerol modulates water permeation through GlpF in the glycerol concentration range around the dissociation constant.

In order to produce an accurate chemical-potential profile of glycerol, I conducted a total of 899 ns equilibrium and non-equilibrium molecular dynamics (MD) simulations, which amounts to about 10 times the computing efforts invested on GlpF in a published work of the current literature. The non-equilibrium MD simulations include three sets of steered molecular dynamics (SMD) [35–37] runs and two MD runs under pressure gradients. The accuracy of the PMF estimation was ascertained by the agreement between the non-equilibrium SMD approach and the equilibrium adaptive biasing force (ABF) approach [24,38].

Glycerol is found to have a deep chemical-potential well in the GlpF channel near the Asn-Pro-Ala (NPA) motifs that is 6.5 kcal/mol below its chemical potential in the bulk of periplasm/cytoplasm. Glycerol binding to or dissociating from this binding site strongly modulates water permeation through the GlpF pore. There are two chemical-potential barriers separating the glycerol binding site from the periplasm and cytoplasm bulk regions; The barrier at the selectivity filter (SF) between the binding site and the periplasm is 10.1 kcal/mol, and the barrier between the NPA and the cytoplasm stands at 4.6 kcal/mol above the bottom of the chemical-potential well. This profile, considered in the context of the structural characteristics of GlpF, leads to a new theory of glycerol modulated water permeation through GlpF that is in full agreement with the *in vitro* results in the current literature. It also harmonizes the existent theoretical results at 0 M glycerol concentration with the *in vitro* experiments at up to 100 mM concentrations of glycerol. Furthermore, it

could be fully validated by future in vitro experiments measuring the glycerol-GlpF dissociation constant and the water permeability in the μM range of glycerol concentration.

2. Methods

2.1. System setup

This study was based on the following all-atom model of GlpF in the cell membrane (Fig. 1): The GlpF tetramer, formed from the crystal structure (PDB code: 1FX8) with 12 glycerols, was embedded in a patch of fully hydrated palmitoyloleylphosphatidyl-ethanolamine (POPE) bilayer. The GlpF-POPE complex is sandwiched by two layers of water, each of which is approximately 30 Å in thickness. The system is neutralized and ionized with Na^+ and Cl^- ions at a concentration of 111 mM. The entire system, consisting of 150,855 atoms, is 114 Å × 115 Å × 112 Å in dimension when fully equilibrated. This system (SysI) has a glycerol concentration of 14 mM. A second system (SysII), for 0 M glycerol, was derived from SysI by deleting all 12 glycerols. It has 150,687 atoms in all and dimensions approximately equal to those of SysI. The Cartesian coordinates are chosen such that the origin is at the geometric center of the GlpF tetramer. The *xy*-plane is parallel to the lipid–water interface and the *z*-axis is pointing from the periplasm to the cytoplasm.

All the simulations of this work were performed using NAMD 2.8 [39]. The all-atom CHARMM36 parameters [40,41] were adopted for all the inter- and intra-molecular interactions. Water was represented explicitly with the TIP3 model. The pressure and the temperature were maintained at 1 bar and 293.15 K, respectively. The Langevin damping coefficient was chosen to be 5/ps. The periodic boundary conditions were applied to all three dimensions, and the particle mesh Ewald was used for the long-range electrostatic interactions. Covalent bonds of hydrogens were fixed to their equilibrium length. The time step of 2 fs was used for short-range interactions in equilibrium simulations, but 1 fs was used for nonequilibrium runs. The same time step of 4 fs was used for long-range forces in both equilibrium and nonequilibrium simulations. The cut-off for long-range interactions was set to 12 Å with a switching distance of 10 Å. In all simulations, the alpha carbons on the trans-membrane helices of GlpF within the range of $-10\ \text{Å} < z < 10\ \text{Å}$ were fixed to fully respect the crystal structure.

2.2. Equilibrium MD

Two runs of 100 ns each in length were conducted for SysI and SysII respectively. Using the theoretical formulation of [42], I computed the mean square displacements (MSD) of the water molecules in the conducting pore. (The MSD curves are shown in supplemental Fig. S1.) The slope of the MSD curve gives an estimate of the osmotic permeabilities of both SysI and SysII that will be presented in the next section.

2.3. Non-equilibrium SMD

SMD runs were conducted to sample the transition paths of glycerol going from the periplasm, through the conducting pore, to the cytoplasm, for computing the 3D PMF of glycerol as a function of its COM position. Three sets of SMD simulations were completed to achieve reliable statistics. (The details are given in the supplemental Figs. S2 to S4.) In each set of SMD, the starting structure is the fully equilibrated structure of SysI. The center of mass of a glycerol was steered/pulled in the positive *z*-direction to sample a forward pulling path, and then pulled in the negative *z*-direction to sample a reverse pulling path. In Set #1 and Set #2, the entire path leading from the periplasm, through the GlpF pore, to the cytoplasm bulk region, was divided into four sections: one section in the periplasm, one section in the cytoplasm, and two sections in the single-file region of the conducting pore. In Set #3, the path through the conducting pore was divided into 19 sections, each 1 Å in

width. Four forward paths and four reverse paths were sampled in each section of Set #1 and the same were done in Set #2. Ten forward paths and ten reverse paths were sampled in each section of Set #3. In all three sets, 4 ns equilibration was performed at both end points of each section so that the pulling paths were sampled between equilibrium states with the glycerol's center-of-mass coordinates being fixed at desired values. And, in all cases, the pulling speed was v = 2.5 Å/ns. It should be noted that the pulling of glycerol's COM was implemented in the single-file vs non-single-file regions with one subtle but important difference: In the single-file region inside the conducting pore, the *z*-coordinate of the glycerol COM was advanced with the constant velocity given above while the *x*- and y-coordinates were not pulled. The *x*- and *y*-degrees of freedom obey the system's dynamics. Thus the *x*- and y-coordinates fluctuates around the potential energy minimum on the *xy*-plane at a given z-coordinate. The COM of glycerol approximately follows the most probable path as it is pulled in the z-direction. In the non-single-file regions from the channel entry vestibule to the periplasm bulk and from the channel exit to the cytoplasm bulk, the z-coordinate was advanced in the same manner as in the single-file region but the *x*- and *y*-degrees of freedom were not left uncontrolled. They were, instead, fixed to their constant values respectively. Otherwise, the glycerol would certainly wander away from the channel axis [43,44].

Along each forward pulling path from A to B, the work done to system was recorded as $W_{A\to Z}$ when glycerol was pulled from A to Z. Along each reverse pulling path from B to A, the work done to system was recorded as $W_{B\to Z}$ when glycerol was pulled from B to Z. Here Z represents a state of the system when the COM *z*-coordinate of the pulled glycerol is z. A and B represent two end states of a given section, respectively. The 1D PMF of glycerol, $G_{1D}(z)$, when its center of mass is at a given coordinate *z*, can be computed through the Brownian dynamics fluctuation-dissipation theorem (BD-FDT) as follows [27,37]:

$$G_{1D}(z) - G_{1D}(z_A) = -k_B T \ln\left(\frac{\langle \exp[-W_{A\to Z}/2k_B T]\rangle_F}{\langle \exp[-W_{Z\to A}/2k_B T]\rangle_R}\right). \quad (1)$$

Here $W_{Z\to A} = W_{B\to A} - W_{B\to Z}$ is the work done to the system for the part of a reverse path when the glycerol was pulled from Z to A. k_B is the Boltzmann constant and T is the absolute temperature. z_A and z_B are the *z*-coordinates of the COM of the pulled glycerol at the end states A and B of the system, respectively. The 3D PMF of glycerol, $G_{3D}(x,y,z)$, when its center of mass is at a given position (x,y,z), can also be computed with BD-FDT:

$$G_{3D}(x,y,z) - G_{3D}(x_A,y_A,z_A) = -k_B T \ln\left(\frac{\langle \exp[-W_{A\to Z}/2k_B T]\rangle_F}{\langle \exp[-W_{Z\to A}/2k_B T]\rangle_R}\right) \quad (2)$$

when the pulling are conducted along a straight line or a fixed curve. Note that only the *z*-components of the pulling forces were necessary for computing the work done to the pulled molecule in both the single-file and the non-single-file regions because the *x*- and y-coordinates were either not pulled or not allowed any displacements. In both cases, only the z-components contribute to the work done.

2.4. 3D PMF to 1D PMF

From the 3D PMF, one can calculate the 1D PMF as follows:[43,44]

$$G_{1D}(z) = -k_B T \ln\left(\int dx dy \exp[-G_{3D}(x,y,z)/k_B T]/A_{\mathbf{ref.}}\right) = G_{3D}(x^*(z), y^*(z), z) - k_B T \ln(A(z)/A_{\mathbf{ref.}}). \quad (3)$$

where $A_{\mathbf{ref}}$ and $A(z)$ are, respectively, the area for reference and the area occupied by the center of mass of glycerol on the plane of a given z-coordinate. $x^*(z)$ and $y^*(z)$ are the median coordinates of integration on the same plane. The second term of the second line of Eq. (3) is the entropic penalty. This term is proportional to the temperature. It does modify the overall rate of transport but does not alter the Arrhenius activation barrier. Inside the single file region $(z_1 < z < z_2)$, the median coordinates of integration $x^*(z)$ and $y^*(z)$ are equal to the coordinates of the minimum of the 3D PMF on the xy-plane, assuming Gaussian approximation. The boundaries of the single-file region are chosen as $z_1 \simeq -7.5$Å and $z_2 \simeq 11.5$ Å respectively. The pore radius is approximately 2 Å at both boundaries (Fig. 2). Taking $A_{\text{ref.}}$ as $A(z_1)$, we have the following approximation for the 3D PMF along the most probable path,

$$G_{3D}(x^*(z), y^*(z), z) = G_{1D}(z) + k_B T \ln(A(z)/A(z_1)) \quad (4)$$

where the area ratio can be evaluated by computing the determinant of the variance matrix of the COM x- and y-coordinates of the glycerol,

$$A(z)/A(z_1) = \left(\begin{vmatrix} \langle \delta x^2 \rangle_z & \langle \delta x \delta y \rangle_z \\ \langle \delta x \delta y \rangle_z & \langle \delta y^2 \rangle_z \end{vmatrix} \Big/ \begin{vmatrix} \langle \delta x^2 \rangle_{z_1} & \langle \delta x \delta y \rangle_{z_1} \\ \langle \delta x \delta y \rangle_{z_1} & \langle \delta y^2 \rangle_{z_1} \end{vmatrix} \right)^{1/2} \quad (5)$$

Here $\delta x = x - x^*(z)$ and $\delta y = y - y^*(z)$ denote deviations from the most probable path. The brackets with subscript z mean the statistical average on the xy-plane of a given z coordinate. Within the margin of error,

$$G_{3D}(x^*(z), y^*(z), z) \simeq G_{1D}(z). \quad (6)$$

Note that the pore radius of the GlpF channel varies between 1.5 Å and 2.5 Å. Approximating the area as proportional to the square of the pore radius, we have

$$-0.35 \text{ kcal/mol} < k_B T \ln[A(z)/A(z_1)] < 0.27 \text{ kcal/mol} \quad \text{for } z_1 < z < z_2. \quad (7)$$

The difference between the 3D and 1D PMFs is smaller than the error bar.

2.5. Computing the dissociation constant

Following Ref. 43, we have the binding constant.

$$c_0/k_d = c_0 \iiint_{\substack{\text{where glycerol} \\ \text{blocks channel}}} dx dy dz \exp[-G_{3D}[x,y,z]/k_B T] = c_0 A(z_1) \int_{-7.5}^{14.5} dz \exp[-G_{1D}[z]/k_B T]. \quad (8)$$

In Eq. (8), $c_0 = 1M = 6.02 \times 10^{-4}\text{Å}^{-3}$ is the standard concentration. k_d is the dissociation constant. The PMF in the bulk is chosen to be zero. The integration is over the region of (-7.5 Å $< z <$ 14.5 Å) where the presence of a glycerol actually occludes the channel for water permeation.

2.6. Accuracy confirmed with ABF approach

In order to ascertain the accuracy of the PMF determined in the BD-FDT approach, I applied the mature ABF method [24,38] to obtained 1D PMF in two 1 Å-wide windows (-5.5 Å $< z < -4.5$ Å and -4.5 Å $< z < -3.5$ Å). A 20 ns MD run and a 90 ns MD run were carried out for the two windows respectively so that convergence was achieved in each window. (The results are shown in the supplemental Figs. S5 and S6 respectively.) These confirm the accuracy of the chemical-potential profile in Fig. 2. Note that the ABF method, an equilibrium sampling approach, is distinctive in nature from the BD-FDT, a non-equilibrium sampling method. Yet, the two approaches produced identical results when long enough MD runs were conducted.

2.7. Non-equilibrium MD under pressure gradients

All the conditions were identical to the equilibrium MD runs of SysI except that the waters (not glycerols) within the conducting pore were subject to a constant force acting on their centers of mass. Those waters have their coordinates within the following range:

$$8\,\mathring{A} < |x| < 20\,\mathring{A}, 8\,\mathring{A} < |y| < 20\,\mathring{A}, |z| < 10\,\mathring{A}. \quad (9)$$

Starting from the end state of the equilibrium MD run of SysI, a 4 ns run was conducted under the afore-described force in the z-direction and the same was done for the negative z-direction.

3. Results and discussion

3.1. Chemical-potential profile of glycerol

Shown in Fig. 2 is the 3D PMF of glycerol as a function of its COM position along a path leading from the periplasm to the entry vestibule of GlpF, through the channel, to the cytoplasm. Inside the channel, waters and glycerols line up in a single file, occluding one another from occupying the same z-coordinate. Outside the channel, farther away from the protein, there is more and more space for multiple waters and glycerols to occupy the same z-coordinate. In the single-file region, the 3D PMF is approximately along the most probable path (minimal free-energy path, plotted in red in Fig. 2). In the non-single-file regions, the chemical potential curves (green) in Fig. 2 are along two straight lines leading from the periplasm to the channel entrance and from the channel exit to the cytoplasm. Integrating the 3D PMF over the channel space [43], we obtain the dissociation constant of glycerol from GlpF as $k_d = 1/\iiint dxdydz \exp[-G_{3D}(x,y,z)/k_BT] \sim 351$ μM. It should be emphasized that the binding site is in the single-file region. Therefore, water permeation through GlpF is modulated by the glycerol concentration in the μM range because a glycerol bound inside GlpF occludes the conducting channel. The inhibitory concentration at half maximum (IC_{50}) is approximately 351 μM. Direct validation of this theory will require *in vitro* measurements of the dissociation constant of the glycerol-GlpF complex, which is currently unavailable in the literature. However, there are *in vitro* data available that validate the biophysical implications of this theory. Discussed below are six implications of the 3D PMF profile given in Fig. 2.

3.1.1. First, binding sites of glycerol in GlpF's pore—The 3D PMF landscape (Fig. 2, top panel) corresponds well with the pore radius of GlpF along the channel (Fig. 2, middle and bottom panels). Where there is a maximum in pore radius, there is a minimum in chemical potential. There are three chemical-potential minima in the single-file region—one in the SF region and two in the NPA region. The locations of these minima are in agreement of the structural studies of GlpF that show a glycerol at the SF and another at the NPA [17,18]. The two minima near the NPA are both far below the bulk chemical-potential level (< − 5 kcal/mol). They are separated from one another by a very low barrier (<3 kcal/mol) and, therefore, a glycerol bound inside the GlpF pore can traverse the region of 2 Å < z < 7 Å rather freely. The minimum at the SF (z = −4 Å) is above the bulk chemical-potential level and it is rather shallow. The barrier separating this minimum from the periplasm is only 2.5 kcal/mol. Dissociation of a glycerol bound at the SF is expected to be within nanoseconds and, indeed, it was observed so in the equilibrium MD simulation. It should be noted that [21] already gave a PMF curve with minima at the SF and NPA that correspond to the binding sites of glycerol determined in the structural study of [17]. However, in terms of glycerol modulating water permeation, the IC_{50} based on their PMF curve would be 24 mM, which is inconsistent with the *in vitro* study of [13] that the presence of up to 100 mM glycerol did not affect the kinetics of water transport.

3.1.2. Second, activation barrier for glycerol permeation—The glycerol permeation rate was measured at multiple temperatures that gave an Arrhenius activation barrier of 9.6 ± 1.5 kcal/mol [13]. This corresponds precisely to the chemical-potential barrier at the SF that is 10.1 ± 1.2 kcal/mol above the bottom of the chemical-potential well near the NPA. It should be noted that the agreement between this theoretical result and the *in vitro* data comes directly, without any adjustments, from the *in silico* experiments based on the all-atom CHARMM36 force field [40]. Earlier, [21] and [24] also produced similar activation barriers for glycerol permeation in their *in silico* studies. Interestingly, the *Plasmodium falciparum* aquaporin (PfAQP) was found to have a similar activation barrier for glycerol transport[45].

3.1.3. Third, activation barrier for water permeation—In the bound state, a glycerol molecule resides in the single-file region, deep inside GlpF's conducting channel, occluding waters or other glycerols from traversing the channel. When the glycerol concentration is in the mM range (far above the dissociation constant, 351 μM), the GlpF pore is practically saturated with glycerol. Water permeation is fully correlated with the glycerol dissociation. Therefore, the Arrhenius barrier for water permeation through GlpF at mM glycerol concentrations is no less than the activation barrier for glycerol dissociation to the cytoplasm (6.5 kcal/mol). This theoretical result of the activation barrier is in agreement with the in vitro data of 7 kcal/mol derived from measurements of the water permeation rates at multiple temperatures [13] if one assumes that the glycerol concentration in the in vitro experiments was significantly higher than the IC_{50} of 351 μM. Indeed, glycerol was used in the experiments of [13]. The 0 mM end of their glycerol concentration range (up to 100 mM) can be higher than 351 μM. At 0 μM glycerol concentration, GlpF's conducting pore will be glycerol-free. The PMF of water permeation was determined to be flat throughout the open channel, having a low Arrhenius barrier, $E_a^0 < 4\ \mathrm{kcal/mol}$ [20,27,31], similar to that of AQPZ [14].

3.1.4. Fourth, water permeation rates through glycerol-free vs. glycerol-saturated GlpF—*In vitro* experiments demonstrated that the water permeation rate in the range of glycerol concentration up to 100 mM was much lower than the water-specific aquaporins (including AQPZ) [13,14,30], but theoretical studies showed that the rate of water permeation through GlpF in absence of glycerols is similar to or greater than through

AQPZ [23,31]. This puzzling point actually serves to validate our theory: Water permeation through glycerol-bound GlpF is much slower than through apo GlpF because a glycerol bound inside GlpF's conducting channel occludes waters and the dissociation of this bound glycerol is a much slower process than that of a water traversing the glycerol-free channel of GlpF. However, as pointed out in Refs. [23,31], the permeation rate measurements are directly related to the reconstitution efficiencies in experiments that are often difficult to control [14]. In contrast, the Arrhenius activation barrier is independent of the reconstitution efficiency. Agreement between its theoretical value and the in vitro results gives a higher degree of certainty than comparing the permeation rate values. Nevertheless, I conducted two equilibrium MD simulations of 100 ns each to compute the rates of water permeation through GlpF with 0 M and 14 mM glycerol concentrations, respectively. The osmotic permeability of water at 0 M glycerol concentration was computed to be $(11 \pm 1) \times 10^{-14} cm^3/s$, which is in agreement with other MD studies in the current literature [23]. And the osmotic permeability at 14 mM glycerol concentration was found to be $(1.5 \pm 0.2) \times 10^{-14} cm^3/s$, which is consistent with the in vitro findings [16], assuming that the glycerol concentration in their experiments was much higher than the IC_{50} of 351 μM based on their use of glycerol during the experiments.

3.1.5. Fifth, concentration-dependence—There is currently no *in vitro* data of the water permeation rate in the μM range of glycerol concentration. Functional experiments in this concentration range are expected to demonstrate significant variation in the water permeation rate from the glycerol-free limit to the glycerol-saturated limit.

3.1.6. Sixth, direction-dependence of water permeation—The glycerol PMF landscape is asymmetrical between the cytoplasmic and the periplasmic sides. This does not mean that there is asymmetry in glycerol transport [22] but it may imply that high glycerol concentrations can make water permeation through GlpF direction-dependent: Permeation from the periplasm to the cytoplasm has an Arrhenius activation barrier of 6.5 kcal/mol while permeation from the cytoplasm to the periplasm has a barrier of 10.1 kcal/mol. A glycerol molecule bound inside the GlpF practically occludes water permeation from the cytoplasm to the periplasm, making water permeation through saturated GlpF directional. In order to explicitly test this possibility, I conducted two nonequilibrium MD simulations of SysI in which the waters in and within the vicinity of the conducting pore are subject to a pressure gradient. Under a pressure-induced force field of 0.01 kcal/mol.Å.amu in the positive *z*-direction, water permeation flow was observed at 50 events/ns, on the average, through each channel. Under the force field of the same magnitude but in the negative *z*-direction, no water permeation events were observed within 4 ns. It should be pointed out that these two nonequilibrium MD simulations cannot be taken as quantitatively accurate because the applied pressure is many orders of magnitude above a realistic osmotic pressure in a biological system. However, they may correctly point to the asymmetry of water permeation at high glycerol concentrations. Another point worth noting is that an imbalance in glycerol concentrations between the periplasm and the cytoplasm may have measurable effects on the water permeation through GlpF as well.

3.2. Relevant interactions

Now, what interactions are responsible for the 3D PMF map shown in Fig. 2? Full understanding has been achieved in regards to the hydrogen-bonding of glycerol/water to the luminal atoms of GlpF throughout its amphipathic pore [17,20,21]. These interactions do not give rise to high barriers or deep wells because the number of hydrogen bonds that a glycerol/water can form with GlpF does not vary drastically with its location throughout the conducting channel. However, the dimension of the conducting pore is not uniform (Fig. 2, middle panel). The narrowest part of the channel is in the SF region, and another narrow part

is between the NPA motifs and the channel exit on the cytoplasmic side. In the region around the NPA motifs, the channel is still single-file in nature but wider than the two narrow regions. Interestingly enough, even the narrowest part of the GlpF channel (3.2 Å in diameter) is wider than the diameter of a water molecule (3 Å). Water can traverse the entire channel without causing structural distortions to the protein. Permeation of water, in the absence of glycerols, is dominated by the hydrogen-bonding interactions among waters and with the luminal atoms. In contrast, the size of a glycerol molecule is 3.6 Å in the least extended dimension. It cannot traverse the GlpF pore as freely as a water molecule can. In fact, it is the close contact between a glycerol molecule and the GlpF lumen that gives rise to the chemical-potential profile shown in Fig. 2. The width of the pore turns out to be such that the van der Waals (VDW) forces on the glycerol by the surrounding residues are all attractive in the NPA region, causing the PMF there to be lower than the bulk level.

Fig. 3(A) shows that, when a glycerol is in the SF region (z = −3.1Å), the narrowest part of the GlpF channel, four residues (Trp 48, Gly 199, Phe 200, and Arg 206) are within the repulsive range (less than 2 Å) of the glycerol. The VDW interactions between these four residues and the glycerol are repulsive, leading to the peak of the VDW energy around z = −3 Å shown in Fig. 3(D).

Fig. 3(B) shows that, when a glycerol is near the NPA motifs (z = 4.0Å), the widest part of the GlpF channel, there are eight residues (Leu 21, Val 52, Leu 67, Asn 68, Leu 159, Ile 187, Met 202, and Asn 203) in the attractive range (between 2 Å and 3 Å) of the glycerol. The attractive VDW interactions between these residues and the glycerol are responsible for the minimum of the VDW energy in the NPA region shown in Fig. 3(D), which ultimately leads to the chemical-potential well in Fig. 2.

Fig. 3(C) shows that, when a glycerol is located in between the NPA and the pore exit (z = 10 Å), the other narrow part of the GlpF channel, there are three residues (Ala 65, His 66, and Leu 67) in the repulsive range (less than 2 Å) of the glycerol. The repulsive VDW interactions between these three residues and the glycerol are weaker than when the glycerol is located near the SF. They show up in Fig. 3(D) as a barrier albeit lower than the one at the SF, and they are ultimately responsible for the barrier in the chemical-potential profile on the cytoplasmic side of the NPA (Fig. 2).

Fig. 3(E) shows the dihedral energy of glycerol as a function of its center-of-mass z-coordinate. Fig. 3(F) and (G) shows the root-mean square deviations of the afore-listed residues from their apo, equilibrium position as functions of the glycerol's center-of-mass z-coordinate. Among the three groups of residues, only the SF-forming residues (Fig. 3(A)) deviate significantly from their apo, equilibrium positions when the glycerol passes by there.

All the factors shown in Fig. 3 combine to demonstrate that the bound state of a glycerol deep inside the GlpF channel owes its existence to the attractive VDW interactions between glycerol and the residues near the NPA motifs. The two chemical-potential barriers result mainly from the repulsive VDW forces on the glycerol by the residues in the two narrow parts of the GlpF channel. The barrier at the SF also has significant contributions from the conformational changes of the SF-forming residues caused by the presence of the glycerol and from the conformational changes of the glycerol itself.

4. Conclusions

Based on the existent *in vitro* experiments and the 3D PMF mapped out in the present study, it is logical to suggest that glycerol bound inside GlpF's conducting channel modulates water permeation through its amphipathic pore. This mechanism explains why GlpF's water-permeability is significantly lower than the water-specific aquaporins and why water

permeation has a large Arrhenius activation barrier when the glycerol concentration is in the mM range. As an addition to the science of hydrogen-bonding of waters and glycerols in the conducting pore, this study demonstrates that the van der Waals interactions between the GlpF and a glycerol play a distinctive biological role. The size of the conducting pore is such that a region exists near the NPA motifs where the VDW interactions between the GlpF and a glycerol are attractive. This precise steric arrangement of GlpF causes the glycerol's chemical potential there to be lower than its bulk level and, therefore, a bound state of glycerol exists deep inside the single-file channel. Finally, it is noted that the IC_{50} of 351 μM is a theoretical estimate which was not directly simulated in this *in silico* study. It needs to be validated with in vitro experiments of measuring the glycerol dissociation constant from GlpF which are not yet available in the current literature.

Supplementary Material

Refer to Web version on PubMed Central for supplementary material.

Acknowledgments

The author acknowledges support from the NIH (Grant #GM084834) and the Texas Advanced Computing Center.

References

1. Agre P, Bonhivers M, Borgnia MJ. The aquaporins, blueprints for cellular plumbing systems. J Biol Chem. 1998; 273(24):14659–14662. [PubMed: 9614059]
2. Borgnia M, et al. Cellular and molecular biology of the aquaporin water channels. Annu Rev Biochem. 1999; 68:425–458. [PubMed: 10872456]
3. Heymann JB, Engel A. Aquaporins: phylogeny, structure, and physiology of water channels. Physiology. 1999; 14(5):187–193.
4. Lee JK, et al. Water and glycerol permeation through the glycerol channel GlpF and the aquaporin family. J Synchrotron Radiat. 2004; 11(1):86–88. [PubMed: 14646142]
5. Agre P, King LS, Yasui M, Guggino WB, Ottersen OP, Fujiyoshi Y, Engel A. Søren Nielsen Aquaporin water channels – from atomic structure to clinical medicine. J Physiol. Jul 1; 2002 542(1):3–16. http://dx.doi.org/10.1113/jphysiol.2002.020818 (Electronic publication ahead of print May 31, 2002). [PubMed: 12096044]
6. Carbrey, JM.; Agre, P. Discovery of the Aquaporins and Development of the Field Aquaporins. Beitz, E., editor. Springer; Berlin Heidelberg: 2009. p. 3-28.
7. Heller KBL, Wilson ECC, Hastings T. Substrate specificity and transport properties of the glycerol facilitator of Escherichia coli. J Bacteriol. 1980; 144(1):5.
8. Zeidel ML, et al. Reconstitution of functional water channels in liposomes containing purified red cell CHIP28 protein. Biochemistry. 1992; 31(33):7436–7440. [PubMed: 1510932]
9. Maurel C, et al. Functional characterization of the Escherichia coli glycerol facilitator, GlpF, in *Xenopus* oocytes. J Biol Chem. 1994; 269(16):11869–11872. [PubMed: 7512955]
10. Walz T, et al. Biologically active two-dimensional crystals of aquaporin CHIP. J Biol Chem. 1994; 269(3):1583–1586. [PubMed: 8294400]
11. Zeidel ML, et al. Ultrastructure, pharmacologic inhibition, and transport selectivity of aquaporin CHIP in proteoliposomes. Biochemistry. 1994; 33(6):1606–1615. [PubMed: 8312280]
12. Yang B, Verkman AS. Water and glycerol permeabilities of aquaporins 1–5 and MIP determined quantitatively by expression of epitope-tagged constructs in *Xenopus* oocytes. J Biol Chem. 1997; 272(26):16140–16146. [PubMed: 9195910]
13. Borgnia MJ, Agre P. Reconstitution and functional comparison of purified GlpF and AqpZ, the glycerol and water channels from *Escherichia coli*. Proc Natl Acad Sci U S A. 2001; 98(5):2888–2893. [PubMed: 11226336]

14. Pohl P, et al. Highly selective water channel activity measured by voltage clamp: analysis of planar lipid bilayers reconstituted with purified AqpZ. Proc Natl Acad Sci U S A. 2001; 98(17):9624–9629. [PubMed: 11493683]
15. Hansen M, et al. A single, bi-functional aquaglyceroporin in blood-stage *Plasmodium falciparum* malaria parasites. J Biol Chem. 2002; 277(7):4874–4882. [PubMed: 11729204]
16. Saparov SM, Tsunoda SP, Pohl P. Proton exclusion by an aquaglyceroprotein: a voltage clamp study. Biol Cell. 2005; 97(7):545–550. [PubMed: 15850456]
17. Fu D, et al. Structure of a glycerol-conducting channel and the basis for its selectivity. Science. 2000; 290(5491):481–486. [PubMed: 11039922]
18. Tajkhorshid E, et al. Control of the selectivity of the aquaporin water channel family by global orientational tuning. Science. 2002; 296(5567):525–530. [PubMed: 11964478]
19. Song J, et al. Molar concentrations of sorbitol and polyethylene glycol inhibit the *Plasmodium* aquaglyceroporin but not thatof E. *coli*: involvement of the channel vestibules. Biochimica et Biophysica Acta (BBA). Biomembranes. 2012; 1818(5):1218–1224.
20. de Groot BL, Grubmüller H. Water permeation across biological membranes: mechanism and dynamics of aquaporin-1 and GlpF. Science. 2001; 294(5550):2353–2357. [PubMed: 11743202]
21. Jensen MØ, et al. Energetics of glycerol conduction through quaglyceroporin GlpF. Proc Natl Acad Sci. 2002; 99(10):6731–6736. [PubMed: 11997475]
22. Lu D, Grayson P, Schulten K. Glycerol conductance and physical asymmetry of the *Escherichia coli* glycerol facilitator GlpF. Biophys J. 2003; 85(5):2977–2987. [PubMed: 14581200]
23. Jensen MØ, Mouritsen OG. Single-channel water permeabilities of *Escherichia coli* aquaporins AqpZ and GlpF. Biophys J. 2006; 90(7):2270–2284. [PubMed: 16399837]
24. Hénin J, et al. Diffusion of glycerol through *Escherichia coli* aquaglyceroporin GlpF. Biophys J. 2008; 94(3):832–839. [PubMed: 17921212]
25. Hub JS, de Groot BL. Mechanism of selectivity in aquaporins and aquaglyceroporins. Proc Natl Acad Sci U S A. 2008; 105(4):1198–1203. [PubMed: 18202181]
26. Chen LY. Free-energy landscape of glycerol permeation through aquaglyceroporin GlpF determined from steered molecular dynamics simulations. Biophys Chem. 2010; 151(3):178–180. [PubMed: 20573441]
27. Chen LY, Bastien DA, Espejel HE. Determination of equilibrium free energy from nonequilibrium work measurements. Phys Chem Chem Phys. 2010; 12(25):6579–6582. [PubMed: 20463999]
28. Oliva R, et al. Electrostatics of aquaporin and aquaglyceroporin channels correlates with their transport selectivity. Proc Natl Acad Sci. 2010; 107(9):4135–4140. [PubMed: 20147624]
29. Chakrabarti N, Roux B, Pomès R. Structural determinants of proton blockage in aquaporins. J Mol Biol. 2004; 343(2):493–510. [PubMed: 15451676]
30. Borgnia MJ, et al. Functional reconstitution and characterization of AqpZ, the *E. coli* water channel protein. J Mol Biol. 1999; 291(5):1169–1179. [PubMed: 10518952]
31. Aponte-Santamaria C, Hub JS, de Groot BL. Dynamics and energetics of solute permeation through the *Plasmodium falciparum* aquaglyceroporin. Phys Chem Chem Phys. 2010; 12(35): 10246–10254. [PubMed: 20607193]
32. Chandler D. Statistical mechanics of isomerization dynamics in liquids and the transition state approximation. J Chem Phys. 1978; 68(6):2959–2970.
33. Kirkwood JG. Statistical mechanics of fluid mixtures. J Chem Phys. 1935; 3(5):300–313.
34. Roux B. Statistical mechanical equilibrium theory of selective ion channels. Biophys J. 1999; 77(1):139–153. [PubMed: 10388746]
35. Isralewitz B, et al. Steered molecular dynamics investigations of protein function. J Mol Graph Model. 2001; 19(1):13–25. [PubMed: 11381523]
36. Park S, Schulten K. Calculating potentials of mean force from steered molecular dynamics simulations. J Chem Phys. 2004; 120(13):5946–5961. [PubMed: 15267476]
37. Chen LY. Exploring the free-energy landscapes of biological systems with steered molecular dynamics. Phys Chem Chem Phys. 2011; 13(13):6176–6183. [PubMed: 21359274]
38. Darve E, Pohorille A. Calculating free energies using average force. J Chem Phys. 2001; 115(20): 9169–9183.

39. Phillips JC, et al. Scalable molecular dynamics with NAMD. J Comput Chem. 2005; 26(16):1781–1802. [PubMed: 16222654]
40. MacKerell AD, Banavali N, Foloppe N. Development and current status of the CHARMM force field for nucleic acids. Biopolymers. 2000; 56(4):257–265. [PubMed: 11754339]
41. Brooks BR, et al. CHARMM: the biomolecular simulation program. J Comput Chem. 2009; 30(10):1545–1614. [PubMed: 19444816]
42. Zhu F, Tajkhorshid E, Schulten K. Collective diffusion model for water permeation through microscopic channels. Phys Rev Lett. 2004; 93(22):224501. [PubMed: 15601094]
43. Allen TW, Andersen OS, Roux B. Molecular dynamics — potential of mean force calculations as a tool for understanding ion permeation and selectivity in narrow channels. Biophys Chem. 2006; 124(3):251–267. [PubMed: 16781050]
44. Zhu F, Hummer G. Theory and simulation of ion conduction in the pentameric GLIC channel. J Chem Theory Comput. 2012; 8(10):3759–3768. [PubMed: 23413364]
45. Chen LY. Glycerol inhibits water permeation through *Plasmodium falciparum* aquaglyceroporin. J Struct Biol. 2013; 181(1):71–76. [PubMed: 23108237]
46. Humphrey W, Dalke A, Schulten K. VMD: visual molecular dynamics. J Mol Graph. 1996; 14(1): 33–38. [PubMed: 8744570]
47. Smart OS, Goodfellow JM, Wallace BA. The pore dimensions of gramicidin A. Biophys J. 1993; 65(6):2455–2460. [PubMed: 7508762]

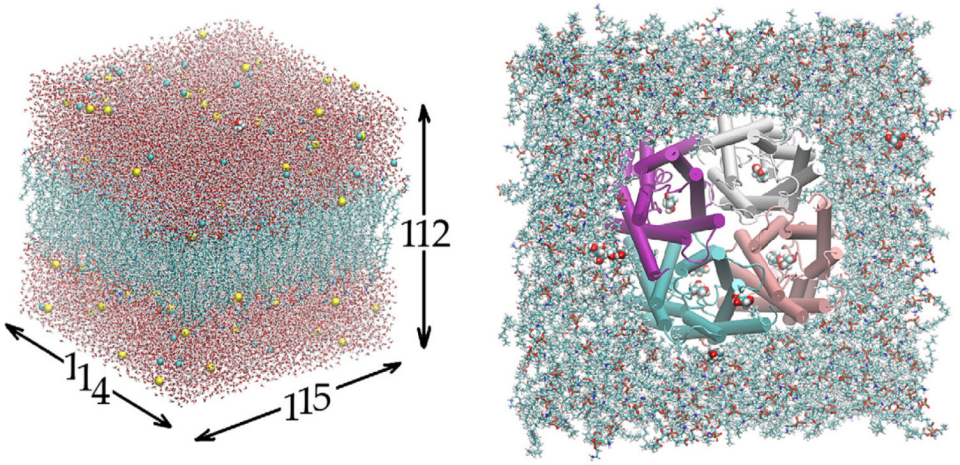

Fig. 1.

All-atom model of GlpF in the cell membrane. The system is 114 Å × 115 Å × 112 Å in dimension. Visible in the left panel are waters (in licorice representation), lipids (licorice), ions (vdw), and one glycerol (vdw). Shown in the right panel are the GlpF tetramer (in cartoon representation, colored by segname), lipids (licorice), and glycerols (vdw). All except GlpF are colored by element name. Graphics rendered with VMD [46].

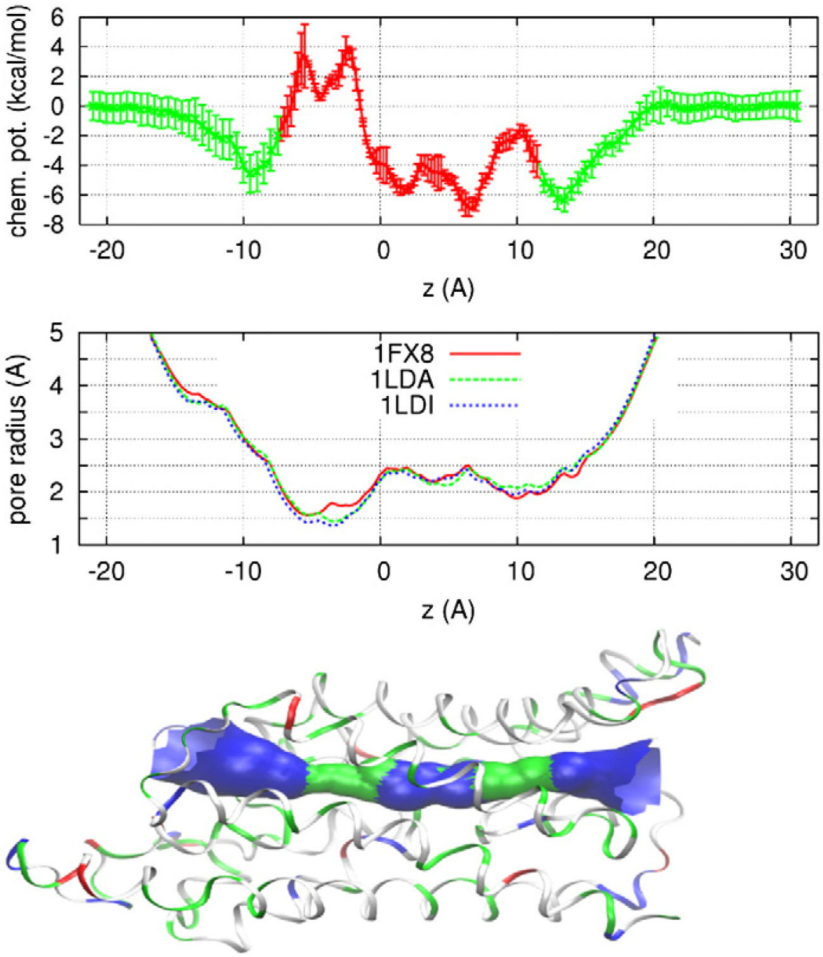

Fig. 2.

The chemical potential (3D PMF) of glycerol as a function of its center-of-mass *z*-coordinate (top panel) where the error bars indicate standard deviation (SD). The pore radius of GlpF crystals (middle panel) from the RCSB Protein Data Bank whose access codes are as shown. The SF region is around $z = -3$ Å and the NPA motifs are located around $z = 4$ Å. The bottom panel illustrates the protein structure (in ribbons, colored with residue type) and the conducting pore of GlpF. Protein structure rendered with VMD [46] and pore radius with HOLE2 [47].

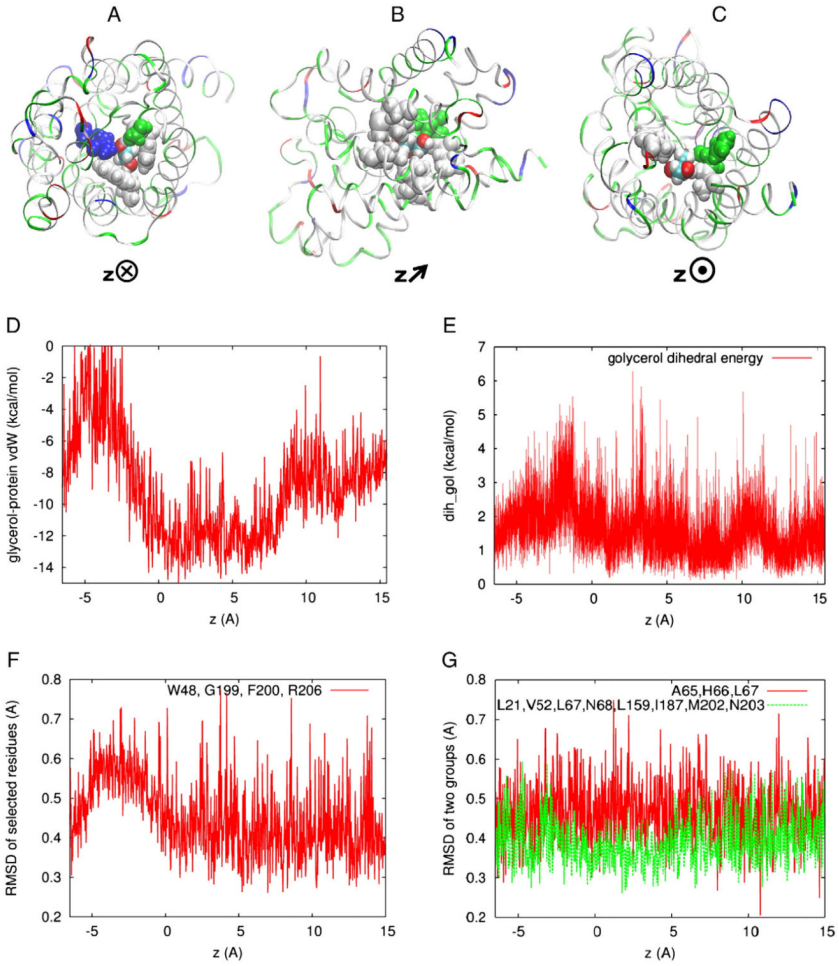

Fig. 3.

The glycerol-GlpF VDW interactions. Top panel, a protomer (in ribbons, colored with residue type) and the glycerol (in vdw, colored with atom name) whose center of mass is located at (A) z = −3.1 Å, (B)z = 4.0 Å, and (C) z = 10 Å respectively. The orientations of the protein are illustrated with the direction of the z-axis pointing (A) into the plane, (B) slanted, and (C) out of the plane. Also shown in the top panel are the relevant residues (in vdw, colored with residue type): (A) Trp 48, Gly 199, Phe 200, and Arg 206 that are in the repulsive range (less than 2 Å) of glycerol, (B) Leu 21, Val 52, Leu 67, Asn 68, Leu 159, Ile 187, Met 202, and Asn 203 that are in the attractive range (between 2 Å and 3 Å) of glycerol, and (C) Ala 65, His 66, and Leu 67 that are in the repulsive range (less than 2 Å) of glycerol. (D) The VDW interaction between a glycerol molecule and GlpF throughout the permeation pore. (E) The di-hedral energy of glycerol as a function of its center-of-mass z-coordinate. (F) The RMSD of selected residues shown in (A) as a function of the glycerol's center-of-mass *z*-coordinate. (G) The same for the residues shown in (B) and (C), respectively. Protein structures rendered with VMD [46].